

Implications of 2dFGRS results on cosmic structure

J.A. Peacock*

*Institute for Astronomy, University of Edinburgh,
Royal Observatory, Edinburgh EH9 3HJ, UK*

Abstract. The 2dF Galaxy Redshift Survey is the first to observe more than 100,000 redshifts, making possible precise measurements of many aspects of galaxy clustering. The spatial distribution of galaxies can be studied as a function of galaxy spectral type, and also of broad-band colour. Redshift-space distortions are detected with a high degree of significance, confirming the detailed Kaiser distortion from large-scale infall velocities, and measuring the distortion parameter $\beta \equiv \Omega_m^{0.6}/b = 0.49 \pm 0.09$. The power spectrum is measured to $\lesssim 10\%$ accuracy for $k > 0.02 h \text{Mpc}^{-1}$, and is well fitted by a CDM model with $\Omega_m h = 0.18 \pm 0.02$ and a baryon fraction of 0.17 ± 0.06 . A joint analysis with CMB data requires $\Omega_m = 0.31 \pm 0.05$ and $h = 0.67 \pm 0.04$, assuming scalar fluctuations. The fluctuation amplitude from the CMB is $\sigma_8 = 0.76 \pm 0.04$, assuming reionization at $z \lesssim 10$, so that the general level of galaxy clustering is approximately unbiased, in agreement with an internal bispectrum analysis. Luminosity dependence of clustering is however detected at high significance, and is well described by a relative bias of $b/b^* = 0.85 + 0.15(L/L^*)$. This is consistent with the observation that L^* in rich clusters is brighter than the global value by 0.28 ± 0.08 mag.

1. AIMS AND DESIGN OF THE 2DFGRS

The 2dF Galaxy Redshift Survey (2dFGRS) was designed to study the following key aspects of the large-scale structure in the galaxy distribution:

- (1) To measure the galaxy power spectrum $P(k)$ on scales up to a few hundred Mpc, bridging the gap between the scales of nonlinear structure and measurements from the the cosmic microwave background (CMB).
- (2) To measure the redshift-space distortion of the large-scale clustering that results from the peculiar velocity field produced by the mass distribution.
- (3) To measure higher-order clustering statistics in order to understand biased galaxy formation, and to test whether the galaxy distribution on large scales is a Gaussian random field.

* *On behalf of the 2dF Galaxy Redshift Survey team:* Matthew Colless (ANU), Ivan Baldry (JHU), Carlton Baugh (Durham), Joss Bland-Hawthorn (AAO), Terry Bridges (AAO), Russell Cannon (AAO), Shaun Cole (Durham), Chris Collins (LJMU), Warrick Couch (UNSW), Gavin Dalton (Oxford), Roberto De Propriis (UNSW), Simon Driver (St Andrews), George Efstathiou (IoA), Richard Ellis (Caltech), Carlos Frenk (Durham), Karl Glazebrook (JHU), Carole Jackson (ANU), Ofer Lahav (IoA), Ian Lewis (AAO), Stuart Lumsden (Leeds), Steve Maddox (Nottingham), Darren Madgwick (IoA), Peder Norberg (Durham), Will Percival (ROE), Bruce Peterson (ANU), Will Sutherland (ROE), Keith Taylor (Caltech).

The survey is designed around the 2dF multi-fibre spectrograph on the Anglo-Australian Telescope, which is capable of observing up to 400 objects simultaneously over a 2 degree diameter field of view. For details of the instrument and its performance see <http://www.aao.gov.au/2df/>, and also Lewis et al. (2002).

The source catalogue for the survey is a revised and extended version of the APM galaxy catalogue (Maddox et al. 1990a,b,c); this includes over 5 million galaxies down to $b_J = 20.5$ in both north and south Galactic hemispheres over a region of almost 10^4 deg^2 (bounded approximately by declination $\delta \leq +3^\circ$ and Galactic latitude $b \gtrsim 20^\circ$). This catalogue is based on Automated Plate Measuring machine (APM) scans of 390 plates from the UK Schmidt Telescope (UKST) Southern Sky Survey. The b_J magnitude system for the Southern Sky Survey is defined by the response of Kodak IIIaJ emulsion in combination with a GG395 filter, and is related to the Johnson–Cousins system by $b_J = B - 0.304(B - V)$, where the colour term is estimated from comparison with the SDSS Early Data Release (Stoughton et al. 2002) The photometry of the catalogue is calibrated with numerous CCD sequences and has a precision of approximately 0.15 mag for galaxies with $b_J = 17\text{--}19.5$. The star-galaxy separation is as described in Maddox et al. (1990b), supplemented by visual validation of each galaxy image.

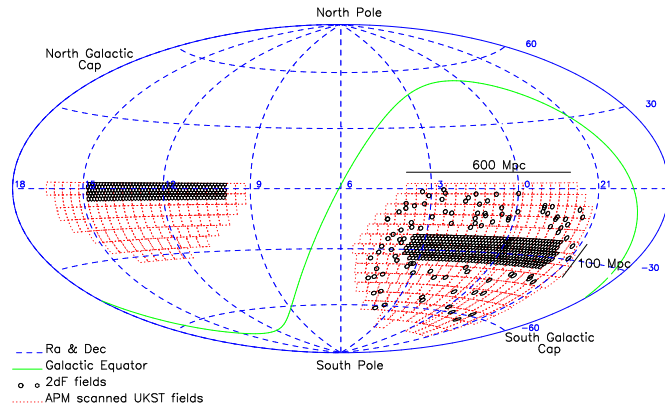


FIGURE 1. The 2dFGRS fields (small circles) superimposed on the APM catalogue area (dotted outlines of Sky Survey plates). There are approximately 140,000 galaxies in the $75^\circ \times 15^\circ$ southern strip centred on the SGP, 70,000 galaxies in the $75^\circ \times 7.5^\circ$ equatorial strip, and 40,000 galaxies in the 100 randomly-distributed 2dF fields covering the whole area of the APM catalogue in the south.

The survey geometry is shown in Figure 1, and consists of two contiguous declination strips, plus 100 random 2-degree fields. One strip is in the southern Galactic hemisphere and covers approximately $75^\circ \times 15^\circ$ centred close to the SGP at $(\alpha, \delta) = (01^h, -30^\circ)$; the other strip is in the northern Galactic hemisphere and covers $75^\circ \times 7.5^\circ$ centred at $(\alpha, \delta) = (12.5^h, +0^\circ)$. The 100 random fields are spread uniformly over the 7000 deg^2 region of the APM catalogue in the southern Galactic hemisphere. At the median redshift of the survey ($\bar{z} = 0.11$), $100 h^{-1} \text{ Mpc}$ subtends about 20 degrees, so the two strips are $375 h^{-1} \text{ Mpc}$ long and have widths of $75 h^{-1} \text{ Mpc}$ (south) and $37.5 h^{-1} \text{ Mpc}$ (north).

The sample is limited to be brighter than an extinction-corrected magnitude of $b_J = 19.45$ (using the extinction maps of Schlegel et al. 1998). This limit gives a good match between the density on the sky of galaxies and 2dF fibres. Due to clustering, however, the number in a given field varies considerably. To make efficient use of 2dF, we employ

an adaptive tiling algorithm to cover the survey area with the minimum number of 2dF fields. With this algorithm we are able to achieve a 93% sampling rate with on average fewer than 5% wasted fibres per field. Over the whole area of the survey there are in excess of 250,000 galaxies.

2. SURVEY STATUS

After an extensive period of commissioning of the 2dF instrument, 2dFGRS observing began in earnest in May 1997, and terminated in April 2002. In total, observations were made of 899 fields, yielding redshifts and identifications for 232,529 galaxies, 13976 stars and 172 QSOs, at an overall completeness of 93%. The galaxy redshifts are assigned a quality flag from 1 to 5, where the probability of error is highest at low Q . Most analyses are restricted to $Q \geq 3$ galaxies, of which there are currently 221,496. An interim data release took place in July 2001, consisting of approximately 100,000 galaxies (see Colless et al. 2001 for details). A public release of the full photometric and spectroscopic database is scheduled for July 2003.

The Colless et al. (2001) paper details the practical steps that are necessary in order to work with a survey of this sort. The 2dFGRS does not consist of a simple region sampled with 100% efficiency, and it is therefore necessary to use a number of masks in order to interpret the data. Two of these concern the input catalogue: the boundaries of this catalogue, including ‘drilled’ regions around bright stars where galaxies could not be detected; also, revisions to the photometric calibration mean that in practice the survey depth varies slightly with position on the sky. A further mask arises from the way in which the sky is tessellated into 2dF tiles: near the survey edges and near internal holes, a lack of overlaps mean that the sampling fraction falls to about 50%. Finally, the spectroscopic success rate of each spectroscopic observation fluctuated according to the observing conditions. The median redshift yield was approximately 95%, but with a tail towards poorer data. The terminal stages of 2dFGRS observing were in fact devoted to re-observing these fields of low completeness; nevertheless, approximately 10% of fields have completeness lower than 80%. This variable sampling makes quantification of the large scale structure more difficult, particularly for any analysis requiring relatively uniform contiguous areas. However, the effective survey ‘mask’ can be measured precisely enough that it can be allowed for in analyses of the galaxy distribution.

3. GALAXY SPECTRA AND COLOURS

Beyond the basic data of positions, magnitudes and redshifts, it is important on physical grounds to be able to divide the 2dFGRS database into different categories of galaxies. This has been done in two different ways. Spectral classification of 2dFGRS galaxies was performed by Folkes et al. (1999) and Madgwick et al. (2002). Principal component analysis was used to split galaxies into a superposition of a small number of templates. Not all of these are robust, owing to uncalibrated spectral distortions in the 2dF instru-

ment, but it was possible to derive a robust classification parameter (termed η) from the templates, which effectively measures the emission-line strength (closely related to the star-formation rate). Galaxies were divided into four spectral classes; their mean spectra and separate luminosity functions are shown in Figure 2.

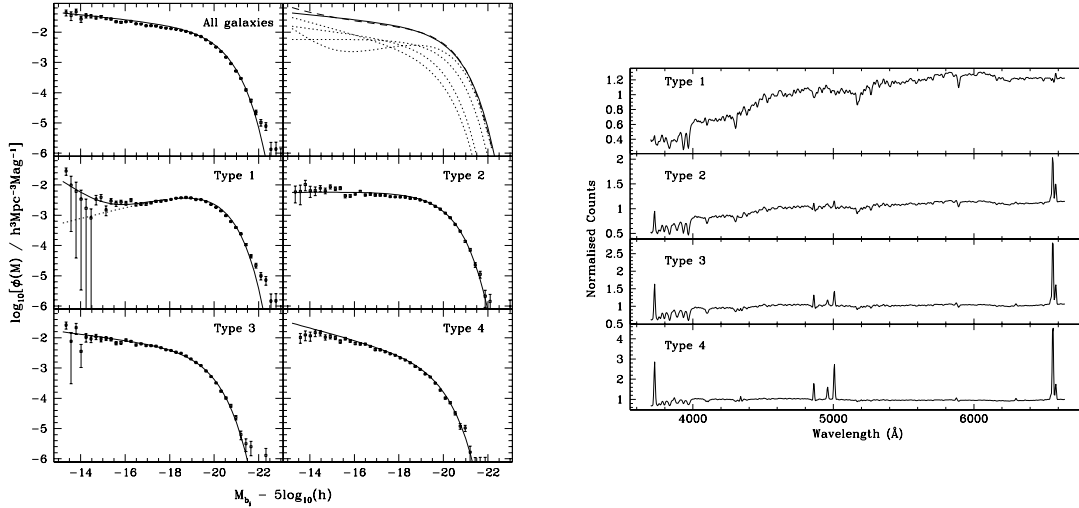


FIGURE 2. The type-dependent galaxy luminosity function according to Madgwick et al. (2002). Principal component analysis was used to split galaxies into a superposition of a small number of templates, and a categorization made based on the decomposition. Type 1 galaxies are generally E/S0, while later types range from Sa to Irr.

This classification method has the drawback that it cannot be used beyond $z = 0.15$, where $H\alpha$ is lost from the spectra. Also, the fibres do not cover the whole galaxy (although Madgwick et al. 2002 show that aperture corrections are not large in practice). More recently, we have been able to obtain total broad-band colours for the 2dFGRS galaxies, using the data from the SuperCOSMOS sky surveys (Hambly et al. 2001). These yield B_J from the same UK Schmidt Plates as used in the original APM survey, but with improved linearity and smaller random errors (0.09 mag rms relative to the SDSS EDR data). The R_F plates are of similar quality, so that we are able to divide galaxies by colour, with an rms in photographic $B - R$ of about 0.13 mag. The systematic calibration uncertainties are negligible by comparison, and are at the level of 0.04 mag. rms in each band. Figure 3 shows that the colour information divides ‘passive’ galaxies with little active star formation cleanly from the remainder, uniformly over the whole redshift range of the 2dFGRS.

As an immediate application, we can display the spatial distribution of 2dFGRS galaxies divided according to colour (Figure 4). The most striking aspect of this image is how closely both sets of galaxies follow the same structure. The passive subset display a more skeletal appearance, as expected owing to morphological segregation of ellipticals. A red-selected survey such as SDSS will appear more similar to the passive subset of the 2dFGRS, with relatively low sampling of the more active spectral type 2–4.

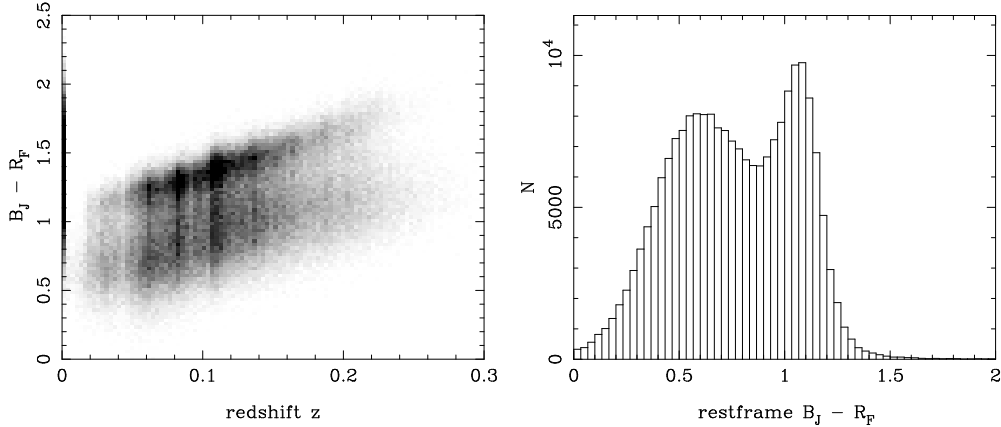


FIGURE 3. Photographic $B - R$ colour versus redshift for the 2dFGRS. The separation between ‘passive’ (red) and ‘active’ (blue) galaxies is very clear. Empirically, $B - R - 2.8z$ defines a ‘restframe’ colour whose distribution is independent of redshift, and very clearly bimodal. This is strongly reminiscent of the distribution of the spectral type, η , and we assume that a division at $(B - R)_0 = 0.85$ achieves a separation of ‘class 1’ galaxies from classes 2–4, as was done using spectra by Madgwick et al. (2002).

4. REDSHIFT-SPACE CORRELATIONS

The simplest statistic for studying clustering in the galaxy distribution is the two-point correlation function, $\xi(\sigma, \pi)$. This measures the excess probability over random of finding a pair of galaxies with a separation in the plane of the sky σ and a line-of-sight separation π . Because the radial separation in redshift space includes the peculiar velocity as well as the spatial separation, $\xi(\sigma, \pi)$ will be anisotropic. On small scales the correlation function is extended in the radial direction due to the large peculiar velocities in non-linear structures such as groups and clusters – this is the well-known ‘Finger-of-God’ effect. On large scales it is compressed in the radial direction due to the coherent infall of galaxies onto mass concentrations – the Kaiser effect (Kaiser 1987).

To estimate $\xi(\sigma, \pi)$ we compare the observed count of galaxy pairs with the count estimated from a random distribution following the same selection function both on the sky and in redshift as the observed galaxies. We apply optimal weighting to minimise the uncertainties due to cosmic variance and Poisson noise. The redshift-space correlation function for the 2dFGRS computed in this way is shown in Figure 5. The correlation-function results display very clearly two signatures of redshift-space distortions. The ‘fingers of God’ from small-scale random velocities are very clear, as indeed has been the case from the first redshift surveys (e.g. Davis & Peebles 1983). However, this is the first time that the large-scale flattening from coherent infall has been seen in detail. An initial analysis of this effect was performed in Peacock et al. (2001), and the final database was analysed by Hawkins et al. (2002).

The degree of large-scale flattening is determined by the total mass density parameter, Ω_m , and the biasing of the galaxy distribution. On large scales, it should be correct to assume a linear bias model, with correlation functions $\xi_g(r) = b^2 \xi(r)$, so that the redshift-space distortion on large scales depends on the combination $\beta \equiv \Omega_m^{0.6}/b$. This is modified by the Finger-of-God effect, which is significant even at large scales and dom-

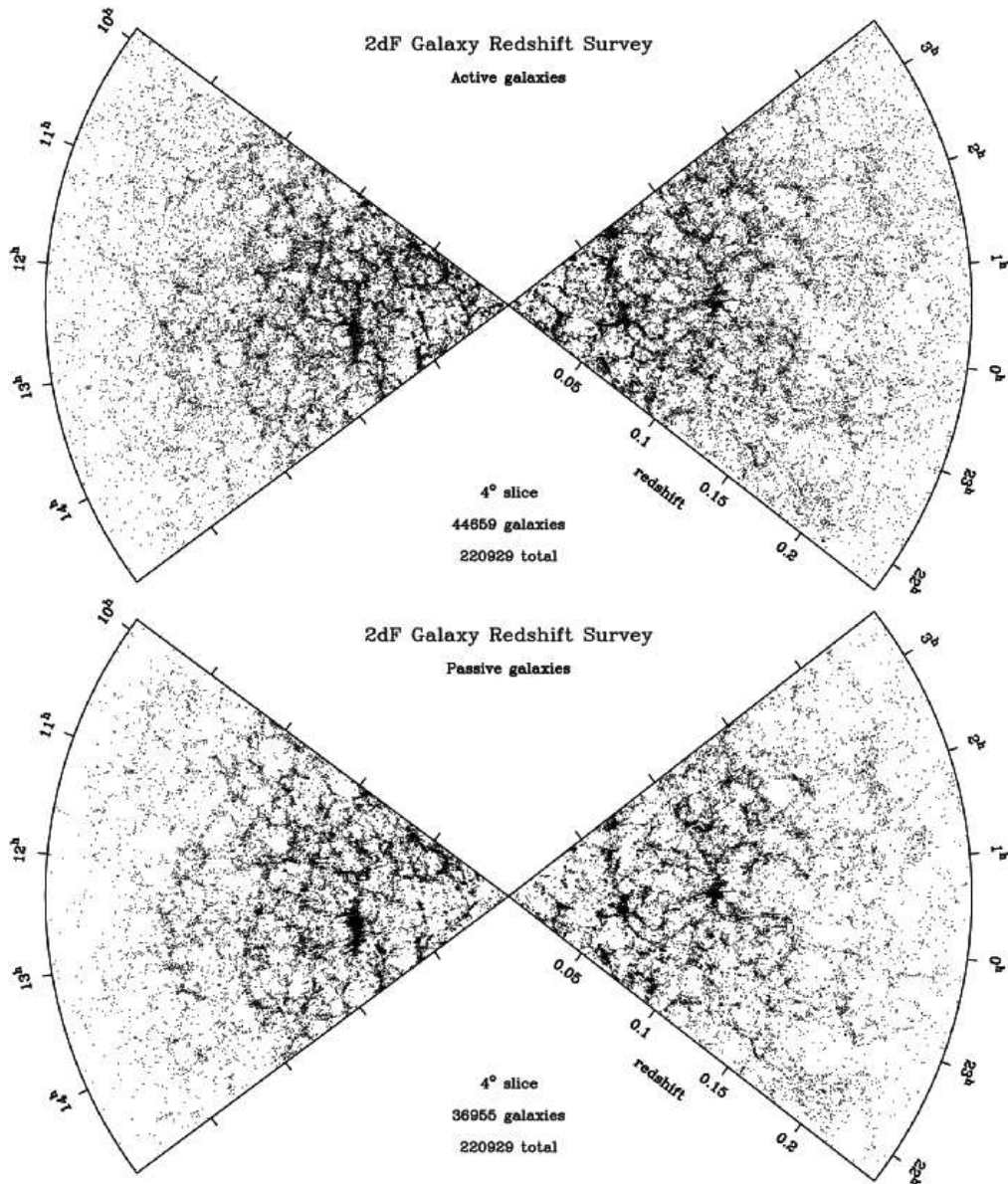


FIGURE 4. The distribution of galaxies in part of the 2dFGRS, drawn from a total of 221,496 galaxies: slices 4° thick, centred at declination -2.5° in the NGP and -27.5° in the SGP. The survey is divided at a rest-frame colour of photographic $B - R = 0.85$, into galaxies with and without active star formation. This image reveals a wealth of detail, including linear supercluster features, often nearly perpendicular to the line of sight. It appears that these transverse features have been enhanced by infall velocities.

inant at small scales. The effect can be modelled by introducing a parameter σ_p , which represents the rms pairwise velocity dispersion of the galaxies in collapsed structures, σ_p (see e.g. Ballinger et al. 1996). Considering both these effects, and marginalising over σ_p , the best estimate of β and its 68% confidence interval according to Hawkins et

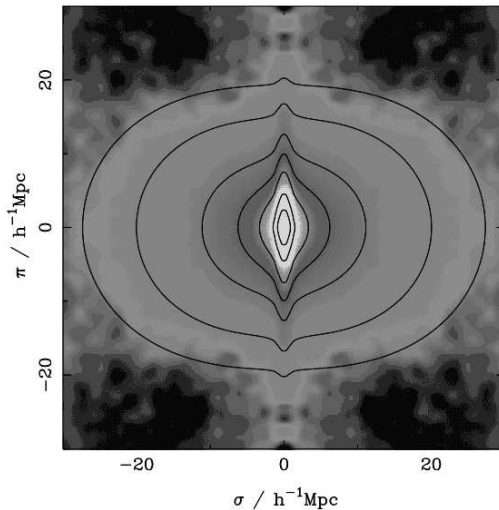


FIGURE 5. The galaxy correlation function $\xi(\sigma, \pi)$ as a function of transverse (σ) and radial (π) pair separation is shown as a greyscale image. It was computed in $0.2 h^{-1}$ Mpc boxes and then smoothed with a Gaussian having an rms of $0.5 h^{-1}$ Mpc. The contours are for a model with $\beta = 0.4$ and $\sigma_p = 400 \text{ km s}^{-1}$, and are plotted at $\xi = 10, 5, 2, 1, 0.5, 0.2$ and 0.1 .

al. (2002) is

$$\beta = 0.49 \pm 0.09 \quad (1)$$

The quoted error is slightly larger than in Peacock et al. (2001): mainly, this reflects the decision of Hawkins et al. to concentrate on the better sampled volume at $z < 0.2$, although a more detailed comparison with mock data also indicates that the previous errors were too small by a factor of about 1.2.

Our measurement of $\Omega^{0.6}/b$ can only be used to determine Ω if the bias is known. We discuss below two methods by which the bias parameter may be inferred, which in fact favour a low degree of bias. Nevertheless, there are other uncertainties in converting a measurement of β to a figure for Ω . The 2dFGRS has a median redshift of 0.11; with weighting, the mean redshift in Hawkins et al. is 0.15, and our measurement should be interpreted as β at that epoch. The optimal weighting also means that our mean luminosity is high: it is approximately 1.4 times the characteristic luminosity, L^* , of the overall galaxy population (Folkes et al. 1999; Madgwick et al. 2002). This means that we need to quantify the luminosity dependence of clustering.

5. REAL-SPACE CLUSTERING AND ITS DEPENDENCE ON LUMINOSITY

The dependence of galaxy clustering on luminosity is an effect that was controversial for a number of years. Using the APM-Stromlo redshift survey, Loveday et al. (1995) claimed that there was no trend of clustering amplitude with luminosity, except possibly at the very lowest luminosities. In contradiction, the SSRS study of Benoist et al.

(1996) suggested that the strength of galaxy clustering increased monotonically with luminosity, with a particularly marked effect for galaxies above L^* . The latter result was arguably more plausible, based on what we know of luminosity functions and morphological segregation. It has been clear for many years that elliptical galaxies display a higher correlation amplitude than spirals (Davis & Geller 1976). Since ellipticals are also more luminous on average, as shown above, some trend with luminosity is to be expected, but the challenge is to detect it.

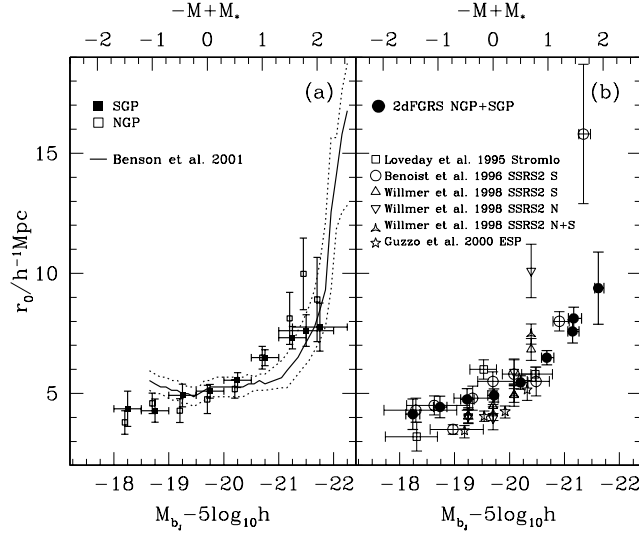


FIGURE 6. (a) The correlation length in real space as a function of absolute magnitude. The solid line shows the predictions of the semi-analytic model of Benson et al. (2001), computed in a series of overlapping bins, each 0.5 magnitudes wide. The dotted curves show an estimate of the errors on this prediction, including the relevant sample variance for the survey volume. (b) The real space correlation length estimated combining the NGP and SGP (filled circles). The open symbols show a selection of recent data from other studies.

The difficulty with measuring the dependence of $\xi(r)$ on luminosity is that cosmic variance can mask the signal of interest. It is therefore important to analyse volume-limited samples in which galaxies of different luminosities are compared in the same volume of space. This comparison was undertaken by Norberg et al. (2001), who measured real-space correlation functions via the projection $\Xi(\sigma) = \int \xi(\sigma, \pi) d\pi$, demonstrating that it was possible to obtain consistent results in both NGP and SGP. A very clear detection of luminosity-dependent clustering was achieved, as shown in Figure 6. The results can be described by a linear dependence of effective bias parameter on luminosity:

$$b/b^* = 0.85 + 0.15 (L/L^*), \quad (2)$$

and the scale-length of the real-space correlation function for L^* galaxies is approximately $r_0 = 4.8 h^{-1} \text{Mpc}$. This trend is in qualitative agreement with the results of Benoist et al. (1996), but in fact these workers gave a stronger dependence on luminosity than is indicated by the 2dFGRS. Finally, with spectral classifications, it is possible to measure the dependence of clustering both on luminosity and on spectral type, to see to what extent morphological segregation is responsible for this result. Norberg

et al. (2002) show that, in fact, the principal effect seems to be with luminosity: $\xi(r)$ increases with L for all spectral types. This is reasonable from a theoretical point of view, in which the principal cause of different clustering amplitudes is the mass of halo that hosts a galaxy (e.g. Cole & Kaiser 1989; Mo & White 1996; Kauffman, Nusser & Steinmetz 1997).

Finally, these results would lead us to infer that the LF must change in strongly clumped regions, shifting to higher luminosities. Such an effect has been sought for many years, but always yielded null results. However, De Propris et al. (2002) have shown that L^* in rich clusters does obey a shift with respect to the global value, being brighter by 0.28 ± 0.08 mag.

6. THE 2DFGRS POWER SPECTRUM

Perhaps the key aim of the 2dFGRS was to perform an accurate measurement of the 3D clustering power spectrum, in order to improve on the APM result, which was deduced by deprojection of angular clustering (Baugh & Efstathiou 1993, 1994). The results of this direct estimation of the 3D power spectrum are shown in Figure 7. This power-spectrum estimate uses the FFT-based approach of Feldman, Kaiser & Peacock (1994), and needs to be interpreted with care. Firstly, it is a raw redshift-space estimate, so that the power beyond $k \simeq 0.2 h \text{Mpc}^{-1}$ is severely damped by fingers of God. On large scales, the power is enhanced, both by the Kaiser effect and by the luminosity-dependent clustering discussed above. Finally, the FKP estimator yields the true power convolved with the window function. This modifies the power significantly on large scales (roughly a 20% correction). We have made an approximate correction for this in Figure 7. The precision of the power measurement appears to be encouragingly high, and the next task is to perform a detailed fit of physical power spectra, taking full account of the window effects. We summarize here results from this analysis (Percival et al. 2001).

The fundamental assumption is that, on large scales, linear biasing applies, so that the nonlinear galaxy power spectrum in redshift space has a shape identical to that of linear theory in real space. We believe that this assumption is valid for $k < 0.15 h \text{Mpc}^{-1}$; the detailed justification comes from analyzing realistic mock data derived from N -body simulations (Cole et al 1998). The model free parameters are thus the primordial spectral index, n , the Hubble parameter, h , the total matter density, Ω_m , and the baryon fraction, Ω_b/Ω_m . Note that the vacuum energy does not enter. Initially, we show results assuming $n = 1$; this assumption is relaxed later.

In order to compare the 2dFGRS power spectrum to members of the CDM family of theoretical models, it is essential to have a proper understanding of the full covariance matrix of the data: the convolving effect of the window function causes the power at adjacent k values to be correlated. This covariance matrix was estimated by applying the survey window to a library of Gaussian realisations of linear density fields. Similar results were obtained using a covariance matrix estimated from a set of mock catalogues. It is now possible to explore the space of CDM models, and likelihood contours in Ω_b/Ω_m versus $\Omega_m h$ are shown in Figure 8. At each point in this surface we have marginalized by integrating the likelihood surface over the two free parameters, h and

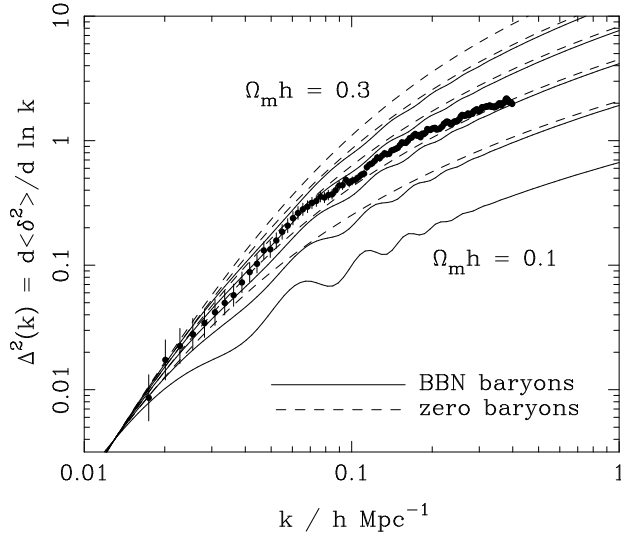


FIGURE 7. The 2dFGRS redshift-space dimensionless power spectrum, $\Delta^2(k)$, estimated according to the FKP procedure. The solid points with error bars show the power estimate. The window function correlates the results at different k values, and also distorts the large-scale shape of the power spectrum. An approximate correction for the latter effect has been applied. The solid and dashed lines show various CDM models, all assuming $n = 1$. For the case with non-negligible baryon content, a big-bang nucleosynthesis value of $\Omega_b h^2 = 0.02$ is assumed, together with $h = 0.7$. A good fit is clearly obtained for $\Omega_m h \simeq 0.2$. Note that the observed power at large k will be boosted by nonlinear effects, but damped by small-scale random peculiar velocities. It appears that these two effects very nearly cancel, but model fitting is generally performed only at $k < 0.15 h \text{ Mpc}^{-1}$ in order to avoid these complications.

the power spectrum amplitude. Assuming a uniform prior for h over a factor of 2 is arguably over-cautious, and we have therefore added a Gaussian prior $h = 0.7 \pm 10\%$. This corresponds to multiplying by the likelihood from external constraints such as the HST key project (Freedman et al. 2001); this has only a minor effect on the results.

Figure 8 shows that there is a degeneracy between $\Omega_m h$ and the baryonic fraction Ω_b/Ω_m . However, there are two local maxima in the likelihood, one with $\Omega_m h \simeq 0.2$ and $\sim 20\%$ baryons, plus a secondary solution $\Omega_m h \simeq 0.6$ and $\sim 40\%$ baryons. The high-density model can be rejected through a variety of arguments, and the preferred solution is

$$\Omega_m h = 0.20 \pm 0.03; \quad \Omega_b/\Omega_m = 0.15 \pm 0.07. \quad (3)$$

The 2dFGRS data are compared to the best-fit linear power spectra convolved with the window function in Figure 8. This shows where the two branches of solutions come from: the low-density model fits the overall shape of the spectrum with relatively small ‘wiggles’, while the solution at $\Omega_m h \simeq 0.6$ provides a better fit to the bump at $k \simeq 0.065 h \text{ Mpc}^{-1}$, but fits the overall shape less well. A preliminary analysis of $P(k)$ from the full final dataset shows that $P(k)$ becomes smoother: the high-baryon solution becomes disfavoured, and the uncertainties narrow slightly around the lower-density solution: $\Omega_m h = 0.18 \pm 0.02$; $\Omega_b/\Omega_m = 0.17 \pm 0.06$.

It is interesting to compare these conclusions with other constraints. These are shown on Figure 8, assuming $h = 0.7 \pm 10\%$. Latest estimates of the Deuterium to Hydrogen

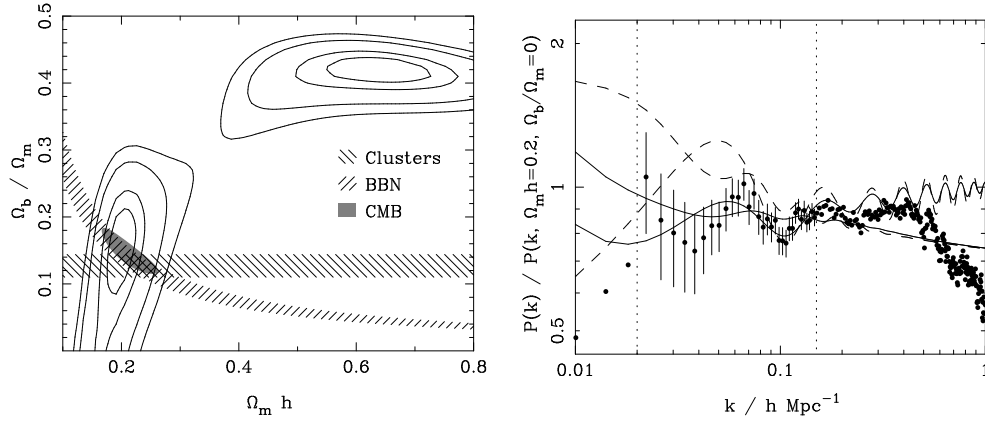


FIGURE 8. Likelihood contours for the best-fit linear power spectrum over the region $0.02 < k < 0.15$. The normalization is a free parameter to account for the unknown large scale biasing. Contours are plotted at the usual positions for one-parameter confidence of 68%, and two-parameter confidence of 68%, 95% and 99% (i.e. $-2 \ln(\mathcal{L} / \mathcal{L}_{\max}) = 1, 2, 3, 6.0, 9.2$). We have marginalized over the missing free parameters (h and the power spectrum amplitude). A prior on h of $h = 0.7 \pm 10\%$ was assumed. This result is compared to estimates from X-ray cluster analysis (Evrard 1997), big-bang nucleosynthesis (Burles et al. 2001) and CMB results (Netterfield et al. 2001; Pryke et al. 2002). The CMB results assume that $\Omega_b h^2$ and $\Omega_{\text{cdm}} h^2$ were independently determined from the data. The second panel shows the 2dFGRS data compared with the two preferred models from the Maximum Likelihood fits convolved with the window function (solid lines). Error bars show the diagonal elements of the covariance matrix, for the fitted data that lie between the dotted vertical lines. The unconvolved models are also shown (dashed lines). The $\Omega_m h \simeq 0.6$, $\Omega_b / \Omega_m = 0.42$, $h = 0.7$ model has the higher bump at $k \simeq 0.05 h \text{Mpc}^{-1}$. The smoother $\Omega_m h \simeq 0.20$, $\Omega_b / \Omega_m = 0.15$, $h = 0.7$ model is a better fit to the data because of the overall shape. A preliminary analysis of the complete final 2dFGRS sample yields a slightly smoother spectrum than the results shown here (from Percival et al. 2001), so that the high-baryon solution becomes disfavoured.

ratio in QSO spectra combined with big-bang nucleosynthesis theory predict $\Omega_b h^2 = 0.020 \pm 0.001$ (Burles et al. 2001), which translates to the shown locus of f_B vs $\Omega_m h$. X-ray cluster analysis predicts a baryon fraction $\Omega_b / \Omega_m = 0.127 \pm 0.017$ (Evrard 1997) which is within 1σ of our value. These loci intersect very close to our preferred model. Moreover, these results are in good agreement with independent estimates of the total density and baryon content from data on CMB anisotropies (e.g. Netterfield et al. 2001; Pryke et al. 2002).

Perhaps the main point to emphasise here is that the 2dFGRS results are not greatly sensitive to the assumed tilt of the primordial spectrum. We have used CMB results to motivate the choice of $n = 1$, as discussed below, but it is clear that very substantial tilts are required to alter the conclusions significantly: $n \simeq 0.8$ would be required to turn zero baryons into the preferred model.

The main residual worry about accepting the above conclusions is probably whether the assumption of linear bias can really be valid. In general, concentration towards higher-density regions both raises the amplitude of clustering, but also steepens the correlations, so that bias is largest on small scales. One way in which this issue can be studied is to use the split by colour introduced above. Figure 9 shows the power spectra for the 2dFGRS divided in this way. The shapes are almost identical (perhaps not so surprising, since the cosmic variance effects are closely correlated in these co-

spatial samples). However, what is impressive is that the relative bias is almost precisely independent of scale, even though the passive subset is rather strongly biased relative to the active subset (relative $b \simeq 1.4$). This provides some reassurance that the large-scale $P(k)$ reflects the underlying properties of the dark matter, rather than depending on the particular class of galaxies used to measure it.

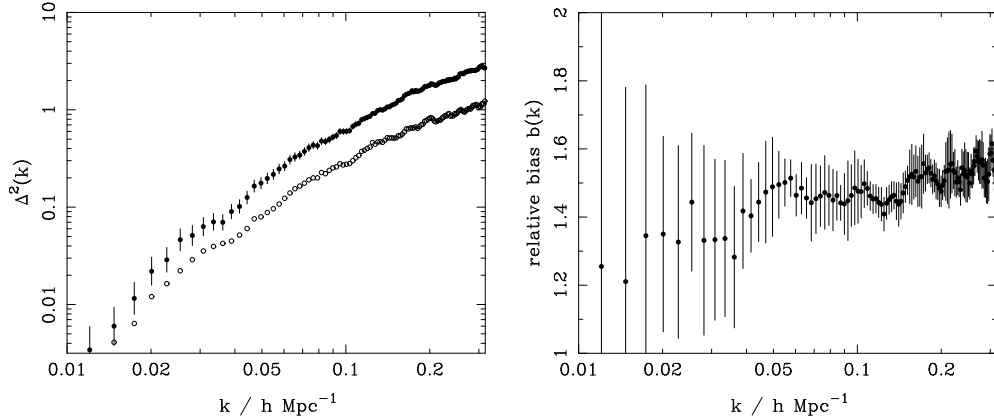


FIGURE 9. The power spectra of passive galaxies (filled circles) and active galaxies (open circles). The shapes are strikingly similar. The square root of the ratio yields the right-hand panel: the relative bias in redshift space of passive and active galaxies. The error bars are obtained by a jack-knife analysis. The relative bias is consistent with a constant value of 1.4 over the range used for fitting of the power-spectrum data ($0.015 < k < 0.15 h \text{Mpc}^{-1}$).

7. COMBINATION WITH THE CMB AND COSMOLOGICAL PARAMETERS

The 2dFGRS power spectrum contains important information about the key parameters of the cosmological model, but we have seen that additional assumptions are needed, in particular the values of n and h . Observations of CMB anisotropies can in principle measure most of the cosmological parameters, and combination with the 2dFGRS can lift most of the degeneracies inherent in the CMB-only analysis. It is therefore of interest to see what emerges from a joint analysis.

These issues are discussed in Efstathiou et al. (2002). The CMB data alone contain two important degeneracies: the ‘geometrical’ and ‘tensor’ degeneracies. In the former case, one can evade the commonly-stated CMB conclusion that the universe is flat, by adjusting both Λ and h to extreme values. In the latter case, a model with a large tensor component can be made to resemble a zero-tensor model with large blue tilt ($n > 1$) and high baryon content. Efstathiou et al. (2002) show that adding the 2dFGRS data removes the first degeneracy, but not the second. This is reasonable: if we take the view that the CMB determines the physical density $\Omega_m h^2$, then a measurement of $\Omega_m h$ from 2dFGRS gives both Ω_m and h separately in principle, removing one of the degrees of freedom on which the geometrical degeneracy depends. On the other hand, the 2dFGRS alone constrains the baryon content weakly, so this does not remove the scope for the tensor degeneracy.

On the basis of this analysis, we can therefore be confident that the universe is very nearly flat ($|\Omega - 1| < 0.05$), so it is defensible to assume hereafter that this is exactly true. The importance of tensors will of course be one of the key questions for cosmology over the next several years, but it is interesting to consider the limit in which these are negligible. In this case, the standard model for structure formation contains a vector of only 6 parameters:

$$\mathbf{p} = (n_s, \Omega_m, \Omega_b, h, Q, \tau). \quad (4)$$

Of these, the optical depth to last scattering, τ , is almost entirely degenerate with the normalization, Q – and indeed with the bias parameter; we discuss this below. The remaining four parameters are pinned down very precisely: using the latest CMB data plus the 2dFRGS power spectrum, we obtain

$$(n_s, \Omega_c h^2, \Omega_b h^2, h) = (0.963 \pm 0.042, 0.115 \pm 0.009, 0.021 \pm 0.002, 0.665 \pm 0.047), \quad (5)$$

or an overall density parameter of $\Omega_m = 0.31 \pm 0.05$.

It is remarkable how well these figures agree with completely independent determinations: $h = 0.72 \pm 0.08$ from the HST key project (Mould et al. 2000; Freedman et al. 2001); $\Omega_b h^2 = 0.020 \pm 0.001$ (Burles et al. 2001). This gives confidence that the tensor component must indeed be sub-dominant. For further details of this analysis, see Percival et al. (2002).

8. MATTER FLUCTUATION AMPLITUDE AND BIAS

The above conclusions were obtained by considering the shapes of the CMB and galaxy power spectra. However, it is also of great interest to consider the amplitude of mass fluctuations, since a comparison with the galaxy power spectrum allows us to infer the degree of bias directly. This analysis was performed by Lahav et al. (2002). Given assumed values for the cosmological parameters, the present-day linear normalization of the mass spectrum (e.g. σ_8) can be inferred. It is convenient to define a corresponding measure for the galaxies, σ_{8g} , such that we can express the bias parameter as

$$b = \frac{\sigma_{8g}}{\sigma_{8m}}. \quad (6)$$

In practice, we define σ_{8g} to be the value required to fit a CDM model to the power-spectrum data on linear scales ($0.02 < k < 0.15 h \text{Mpc}^{-1}$). A final necessary complication of the notation is that we need to distinguish between the apparent values of σ_{8g} as measured in redshift space (σ_{8g}^S) and the real-space value that would be measured in the absence of redshift-space distortions (σ_{8g}^R). It is the latter value that is required in order to estimate the bias.

A model grid covering the range $0.1 < \Omega_m h < 0.3$, $0.0 < \Omega_b / \Omega_m < 0.4$, $0.4 < h < 0.9$ and $0.75 < \sigma_{8g}^S < 1.14$ was considered. The primordial index was assumed to be $n = 1$ initially, and the dependence on n studied separately. For fixed ‘concordance model’ parameters $n = 1$, $k = 0$, $\Omega_m = 0.3$, $\Omega_b h^2 = 0.02$ and a Hubble constant $h = 0.70$,

we find that the amplitude of 2dFGRS galaxies in redshift space is $\sigma_{8g}^S(L_s, z_s) = 0.94$. Correcting for redshift-space distortions as detailed above reduces this to 0.86 in real space. Applying a correction for a mean luminosity of $1.9L^*$ using the recipe of Norberg et al. (2001), we obtain an estimate of $\sigma_{8g}^R(L^*, z_s) = 0.76$, with a negligibly small random error. In order to obtain present-day bias figures, we need to know the evolution of galaxy clustering to $z = 0$. Existing data on clustering evolution reveals very slow changes: higher bias at early times largely cancels the evolution of the dark matter. We therefore assume no evolution in σ_{8g} .

The value of σ_8 for the dark matter can be deduced from the CMB fits:

$$\sigma_8 = (0.72 \pm 0.04) \exp \tau, \quad (7)$$

where the error bar includes both data errors and theory uncertainty. The unsatisfactory feature is the degeneracy with the optical depth to last scattering. For reionization at redshift 8, we would have $\tau \simeq 0.05$; it is unlikely that τ can be hugely larger (e.g. Loeb & Barkana 2001). Although direct removal of this theoretical prejudice is desirable (and will be possible with future CMB data), it seems reasonable to assume that the true value of σ_8 must be very close to 0.76. Within the errors, this agrees perfectly with our $\sigma_{8g}^R(L^*, 0) = 0.76$, implying that L^* galaxies are very nearly exactly unbiased. As we have seen, there are large variations in the clustering amplitude with type, so that this outcome must be something of a coincidence.

Finally, this conclusion of near-unity bias was reinforced in a completely independent way, by using the measurements of the bispectrum of galaxies in the 2dFGRS (Verde et al. 2002). As it is based on three-point correlations, this statistic is sensitive to the filamentary nature of the galaxy distribution – which is a signature of nonlinear evolution. One can therefore split the degeneracy between the amplitude of dark-matter fluctuations and the amount of bias. At the effective redshift and luminosity of their sample ($z_s = 0.17$ and $L = 1.9L^*$), Verde et al. found $b = 1.04 \pm 0.11$. Although the corrections to zero redshift and to luminosity L^* are probably significant, this reinforces the point that on large scales there is no substantial difference in clustering between typical galaxies and the dark matter (small scales, of course, are another matter entirely).

9. CONCLUSIONS

The 2dFGRS is the first 3D survey of the local universe to achieve 100,000 redshifts, almost an order of magnitude improvement on previous work. The final database should yield definitive results on a number of key issues relating to galaxy clustering. For details of the current status of the 2dFGRS, see <http://www.mso.anu.edu.au/2dFGRS>. In particular, this site gives details of the 2dFGRS public release policy, in which approximately the first half of the survey data were made available in June 2001, with the complete survey database to be made public by mid-2003. Some key results of the survey to date may be summarized as follows:

- (1) The galaxy luminosity function has been measured precisely as a function of spectral type (Folkes et al. 1999; Madgwick et al. 2002).

- (2) The amplitude of galaxy clustering has been shown to depend on luminosity (Norberg et al. 2001). The relative bias is $b/b^* = 0.85 + 0.15 (L/L^*)$.
- (3) The redshift-space correlation function has been measured out to $30h^{-1}$ Mpc. Redshift-space distortions imply $\beta \equiv \Omega_m^{0.6}/b = 0.49 \pm 0.09$, for galaxies with $L \simeq 1.4L^*$.
- (4) The galaxy power spectrum has been measured to high accuracy (10–15% rms) over about a decade in scale at $k < 0.15 h \text{Mpc}^{-1}$. The results are very well matched by an $n = 1$ CDM model with $\Omega_m h = 0.18$ and 16% baryons.
- (5) Combining the power spectrum results with current CMB data, very tight constraints are obtained on cosmological parameters. For a scalar-dominated flat model, we obtain $\Omega_m = 0.31 \pm 0.05$, and $h = 0.68 \pm 0.04$, independent of external data.
- (6) Results from the CMB comparison imply a large-scale bias parameter consistent with unity. This conclusion is also reached in a completely independent way via the bispectrum analysis of Verde et al. (2002).

Overall, these results provide precise support for a cosmological model that is flat, with $(\Omega_b, \Omega_c, \Omega_v) \simeq (0.04, 0.25, 0.71)$, to a tolerance of 10% in each figure. Although the Λ CDM model has been claimed to have problems in matching galaxy-scale observations, it clearly works extremely well on large scales, and any proposed replacement for CDM will have to maintain this agreement. So far, there has been no need to invoke either tilt of the scalar spectrum, or a tensor component in the CMB. If this situation is to change, the most likely route will be via new CMB data, combined with the key complementary information that the large-scale structure in the 2dFGRS can provide.

ACKNOWLEDGEMENTS

The 2dF Galaxy Redshift Survey was made possible by the dedicated efforts of the staff of the Anglo-Australian Observatory, both in creating the 2dF instrument, and in supporting it on the telescope.

REFERENCES

- Ballinger W.E., Peacock J.A., Heavens A.F., 1996, MNRAS, 282, 877
 Baugh C.M., Efstathiou G., 1993, MNRAS, 265, 145
 Baugh C.M., Efstathiou G., 1994, MNRAS, 267, 323
 Benoist C., Maurogordato S., da Costa L.N., Cappi A., Schaeffer R., 1996, ApJ, 472, 452
 Benson, A.J., Frenk, C.S., Baugh, C.M., Cole, S., Lacey, C.G., 2001, MNRAS, 327, 1041
 Burles S., Nollett K.M., Turner M.S., 2001, ApJ, 552, L1
 Cole S., Kaiser N., 1989, MNRAS, 237, 1127
 Cole S., Hatton S., Weinberg D.H., Frenk C.S., 1998, MNRAS, 300, 945
 Colless M. et al., 2001, MNRAS, 328, 1039

Davis M., Geller M.J., 1976, ApJ, 208, 13
Davis M., Peebles, P.J.E., 1983, ApJ, 267, 465
De Propris R. et al., 2002, astro-ph/0212562
Efstathiou G. et al., 2002, MNRAS, 330, L29
Evrard A., 1997, MNRAS, 292, 289
Folkes S.J. et al., 1999, MNRAS, 308, 459
Feldman H.A., Kaiser N., Peacock J.A., 1994, ApJ, 426, 23
Freedman W.L. et al., 2001, ApJ, 553, 47
Hambly N.C., Irwin M.J., MacGillivray H.T., 2001, MNRAS 326 1295
Hawkins E.J. et al., 2002, astro-ph/0212375
Kaiser N., 1987, MNRAS, 227, 1
Kauffmann G., Nusser A., Steinmetz M., 1997, MNRAS, 286, 795
Lahav O. et al., 2002, MNRAS, 333, 961
Lewis I.J. et al., 2002, MNRAS, 333, 279
Loeb A., Barkana R., 2001, ARAA, 39, 19
Loveday J., Maddox S.J., Efstathiou G., Peterson B.A., 1995, ApJ, 442, 457
Maddox S.J., Efstathiou G., Sutherland W.J., Loveday J., 1990a, MNRAS, 242, 43P
Maddox S.J., Sutherland W.J., Efstathiou G., Loveday J., 1990b, MNRAS, 243, 692
Maddox S.J., Efstathiou G., Sutherland W.J., 1990c, MNRAS, 246, 433
Madgwick D. et al., 2002, 333, 133
Mo H.J., White S.D.M., 1996, MNRAS, 282, 347
Mould J.R. et al., 2000, ApJ, 529, 786
Netterfield C.B. et al., 2001, astro-ph/0104460
Norberg P. et al., 2001, MNRAS, 328, 64
Norberg P. et al., 2002, MNRAS, 332, 827
Peacock J.A. et al., 2001, Nature, 410, 169
Percival W.J. et al., 2001, MNRAS, 327, 1297
Percival W.J. et al., 2002, MNRAS, 337, 1068
Pryke C. et al., 2002, ApJ, 568, 46
Schlegel D.J., Finkbeiner D.P., Davis M., 1998, ApJ, 500, 525
Stoughton C.L. et al., 2002, AJ, 123, 485
Verde L. et al., 2002, MNRAS, 335, 432